From satellite images to urban-scale air temperatures: A Multi-Layer Perceptron approach

Geunchan Song[1], **Azarakhsh Rafiee**[1] **and Martín Mosteiro-Romero**[1,2]

[1]Faculty of Architecture and the Built Environment, Delft University of Technology, Netherlands
[2]Faculty of Civil Engineering and Geosciences, Delft University of Technology, Netherlands

M.A.MosteiroRomero@tudelft.nl

Abstract -

A detailed understanding of the Urban Heat Island is crucial for energy efficiency, renewable integration, building system automation and demand response in district energy systems. Satellite images provide high resolution information about land surface temperatures (LST) at urban scale, but do not provide information about air temperature (AT), which affect energy performance and thermal comfort. This paper presents a methodology to estimate AT at urban scale for the case of Seoul, South Korea. A Multi-Layer Perceptron (MLP) neural network was developed to convert satellite-derived LST to AT using 12 years of satellite imagery and air temperature measurements from local automatic weather stations (AWS). The method is then independently tested by comparing the predicted temperatures to the measurements from 1000+ distributed "Seoul Data of Things" (S-DoT) sensors in the city. The model was found to achieve an R^2 value of 0.968 during validation using the AWS data from the period 2013–2024. The mean difference during the independent testing was 0.98°C, with an R^2 of 0.807, confirming the model successfully predicts actual air temperatures rather than sensor-specific values.

Keywords -

Urban Heat Island; Air Temperature; Remote Sensing; Multi-Layer Perceptrons

1 Introduction

Rapid urbanization and industrialization have intensified the challenges posed by global warming. As population in cities increases, urban areas have become significant contributors to greenhouse gas emissions while simultaneously experiencing the adverse effects of climate change. Among these effects, the increased air temperature of a city compared to the surrounding rural area, known as the Urban Heat Island (UHI) [1], exacerbates global warming by amplifying energy demands and deteriorating air quality.

A detailed understanding of the UHI in urban areas is crucial for urban planning decisions to support both energy efficiency [2] and renewable integration [3] As urban temperatures increase, space cooling demand increases, with implications on the design and operation of buildings and energy systems. Effective building automation and demand response in district energy systems require accurate load forecasting, where a detailed understanding of the expected air temperatures during operation is crucial. In spite of the considerable effects of the urban environment on local air temperatures, such data is rarely available at sufficient spatial resolution, creating a gap between climate analysis and practical urban energy applications.

1.1 Measuring the UHI

The most direct way to measure the UHI is through weather stations that record air temperature at standard heights within the urban canopy, from ground level to the tops of trees and buildings [4]. However, weather stations have limited spatial coverage, while the effects of the urban climate can be highly localized based on street layout and building materials. Another solution is adding low-cost weather sensors. For example, Schatz and Kucharik [5] installed 150 temperature and humidity sensors at 3.5 meters height on streetlights and utility poles in Madison, USA, to capture fine-scale temperature variations.

One of the most widely used methods for obtaining precise temperature data in UHI studies is using satellite imagery. Satellite imagery can provide a very high spatial coverage of urban land surface temperatures by measuring thermal radiation from surfaces compared to weather stations. Thermal remote sensing has been used for decades to assess the UHI, to perform land cover classifications and in models of urban surface atmosphere exchange [4].

Ground-based weather stations, while providing accurate point measurements, typically offer sparse spatial coverage in urban areas, often one station per several square kilometers. This spatial limitation makes it challenging to capture the fine-scale temperature variations essential for understanding urban heat island effects and their relationships with UFEs at the building or neighborhood scale. Satellite thermal imagery offers complete spatial coverage at resolutions of 30-100m, providing temperature information for every pixel across entire cities. However, satellites measure surface temperature rather than air temperature, necessitating conversion methods to obtain the air temperature values required for building energy analysis and human comfort assessment. Combining these data sources can offer the spatial completeness of satellite data while maintaining relevance to energy consumption patterns and urban planning applications.

1.2 Converting Land Surface Temperature to Air Temperature

The most fundamental approach to obtain urban-scale air temperature from satellite data involves simple linear regression between LST and air temperature [6]. Multiple linear regression (MLR) incorporates additional predictor variables beyond LST to improve accuracy [7]. Chen et al. [8] developed an enhanced empirical regression method that incorporated multiple predictors and achieved an average error within ±2.5K for 98% of weather stations. Another option is Regression Kriging (RK), which applies regression to establish relationships between temperature and auxiliary variables, and kriging to spatially interpolate based on their spatial structure. RK has been successfully implemented to generate temperature maps at high resolution [9]. However, it assumes linear relationships in trend, while temperatures have complicated non-linear relationships, making it infeasible to analyze detailed relationships [10].

Among machine learning methods, Random Forests (RF) have emerged as a powerful method for air temperature estimation [11]. The RF algorithm has a great ability to handle non-linear relationships and multiple variables, making it particularly suitable for complex urban environments. However, RF can create artificial spatial patterns due to its tree-based structure, which may be problematic for continuous temperature mapping. Also, RF significantly underestimates temperature extremes and struggles to recover finer scale spatial resolution.

Neural networks have also been successfully implemented. Choi et al. [12] used Artificial Neural Networks (ANN) and achieved high accuracy, though they noted that model performance is highly dependent on input variables and network architecture. Multi-Layer Perceptron (MLP) neural networks have shown superior performance for air temperature estimation, particularly in challenging conditions [13]. MLP can effectively combine LST with auxiliary variables like NDVI, elevation and solar angles to create comprehensive air temperature maps [7].

While more advanced algorithms and neural network architectures could be explored, MLP was selected in this work due to its robustness, lower data requirements and demonstrated performance in air temperature predictions. MLP produces smooth, continuous temperature surfaces by learning the underlying physical relationships between variables. MLP can capture the non-linear relationships between LST and air temperature that vary with surface types, time of day and weather conditions. The ability to integrate multiple input variables simultaneously is another key strength. MLPs work well with standard table-formatted data and do not need special data structures to perform effectively [14].

1.3 Scope of this paper

This paper presents an MLP-based methodology for the conversion of LSTs from satellite images to air temperatures at urban scale for energy planning and system operation. While many studies have examined the UHI effect and building energy consumption, several research gaps remain in current approaches. Most research analyzes these phenomena over short periods, missing long-term urban transformations and their cumulative impacts [15]. While Raj and Yun [16] analyzed surface UHI effect in Seoul over 20 years using remote sensing, they specifically focused on LST rather than air temperatures. Furthermore, few studies validate their models using independent, spatially dense sensor networks.

These limitations highlight the need for an integrated, long-term approach that can handle complex non-linear relationships while providing practical insights for urban planning. Long-term analysis capturing actual urban transformations, rather than static snapshots, is essential for understanding how development patterns influence environmental outcomes. In this context, this research aims to contribute to these gaps through: (1) the integration of long-term satellite and ground-based datasets over a 12-year period; (2) the use of independent high-density IoT sensor networks (S-DoT) for external validation; and (3) the demonstration of spatially continuous air temperature mapping suitable for urban energy applications. Thus, this research provides a first step towards a more detailed understanding of the UHI in Seoul and its effects on urban energy systems.

2 Methodology

The methodology employs a two-stage approach, as shown in Figure 1. Stage 1 focuses on training the MLP using 39 AWSs data as ground truth. Air temperature measurements at 11:12 AM from 2013 to 2024 are matched with the Landsat 8 overpass time. The MLP model learns the complex non-linear relationships between 4 input variables: Land Surface Temperature (LST), Normalized Difference Vegetation Index (NDVI), Digital Elevation Model (DEM) and Solar Zenith Angle (SZA), and the measured air temperature from AWSs. Stage 2 tests the trained model using independent data from over 1,100 S-DoT sensors across Seoul since 2021. This independent test-

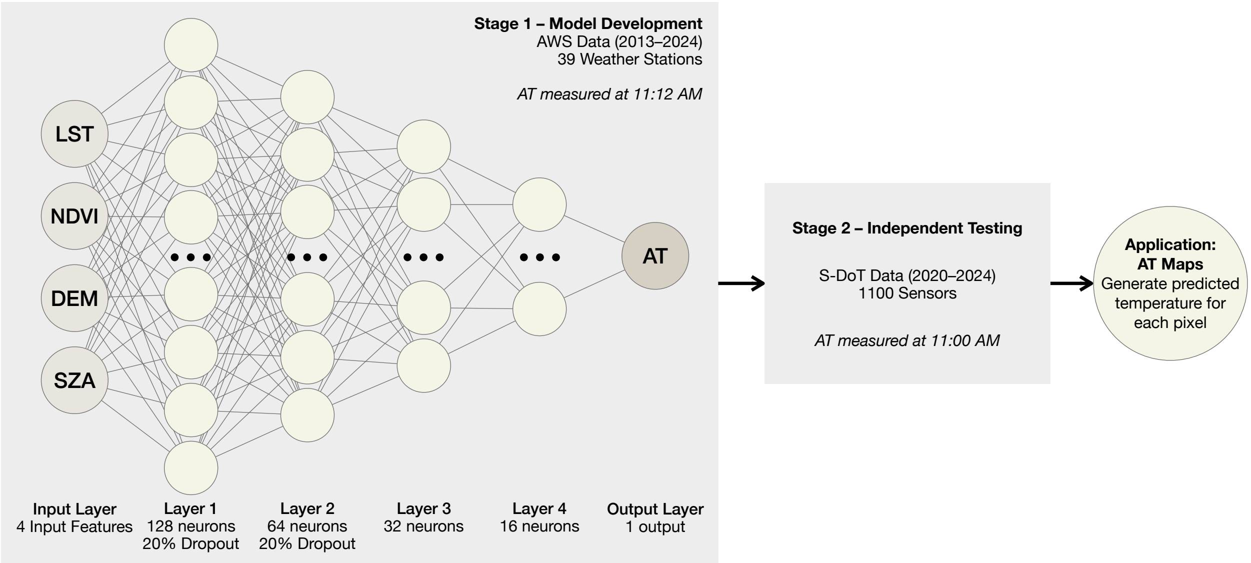

Figure 1. Model development and testing methodology showing the five-layer MLP architecture with dropouts

ing confirms the model's performance on a spatially dense network not used during training.

2.1 Data collection

2.1.1 Satellite data

This research uses Landsat 8 due to its extensive temporal coverage of over 10 years and high spatial resolution of 30 by 30 meters. From Landsat 8, the digital elevation model (DEM) and solar zenith angle (SZA) can be acquired, while LST and normalized difference vegetation index (NDVI) can be calculated using three spectral bands: Band 4 (red), Band 5 (near-infrared, NIR) and Band 10 (Thermal Infrared) [17]. This research uses Google Earth Engine to collect these bands and calculate the LST and NDVI of the research area.

Landsat 8 orbits the Earth every 16 days, which means that the satellite only captures the area 1 or 2 times per month. Seoul is captured at around 11:12 in the morning, which is close to the peak temperature in a day. This temporal limitation means that the model outputs consist of single monthly values derived from these satellite observations at their specific capture times rather than continuous temporal data.

Satellite images from Landsat 8 were collected from March 2013 (the first available month) to December 2024. During this period, 118 images were collected, however not all satellite images from Landsat are useful for temperature calculations. Satellite imagery is very vulnerable to cloud cover, which can obscure most of the land area. Thus, only images where the cloud coverage was less than 30% sky and the research area was fully visible were selected. When no suitable images were available within this threshold for specific time periods, the cloud coverage limit was incrementally increased if acceptable quality images could still be obtained. As a result, we were able to collect 7 valid images per year, which corresponded to 7 valid images per month over the 12-year period of study.

The input features for the MLP model are shown in Fig. 2. Land Surface Temperature (LST) serves as the primary input, providing thermal information measured by Landsat 8 bands at 11:12 AM. The Normalized Difference Vegetation Index (NDVI) represents vegetation greenness, which significantly affects the LST and air temperature relationship through the evapotranspiration process. NDVI values range from -1 to 1, with higher values indicating denser vegetation. The Digital Elevation Model (DEM) represents terrain elevation, affecting air temperature through the environmental lapse rate where temperature decreases approximately 6.5°C per 1000 m elevation gain. Elevation influences wind exposure and cold air pooling, making it an essential predictor for temperature estimation. Finally, the Solar Zenith Angle (SZA) represents the angle between the sun and the vertical direction, which determines the intensity of solar radiation. It influences the amount of solar radiation reaching the surface, affecting both LST and air temperature.

2.1.2 Weather data

The Korean Meteorological Administration (KMA) operates 554 automatic weather stations (AWSs) throughout the country that record air temperatures, wind speed, pressure and other climatic factors at subhourly scale [18]. Out of these, 28 AWSs are installed in Seoul, shown in Fig. 3. Although the spatial resolution of the AWS is low com-

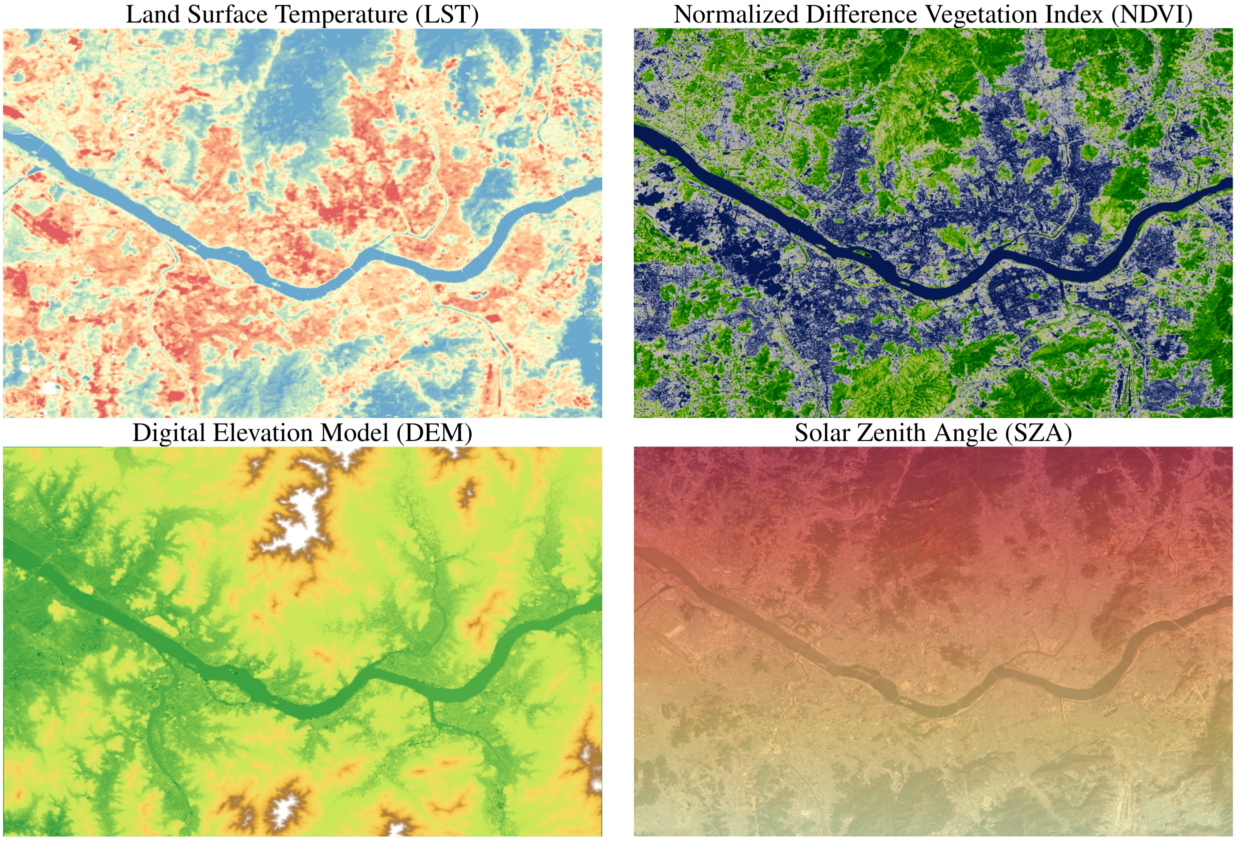

Figure 2. Examples of the four input features in the MLP model

pared to the satellite imagery (28 AWSs in Seoul, which has an area 605.25 km), it has a very high temporal resolution. This research additionally considers 9 AWSs near the Seoul border to increase spatial resolution.

In addition to these weather stations, the Korean government installed weather sensors in 2020 as part of an initiative called Seoul Data of Things (S-DoT). S-DoT is a city data sensor that collects various urban phenomena data, such as fine dust level, temperature, relative humidity, noise, illumination level, ultraviolet radiation, and other parameters at hourly scale [19]. As of 2024, 1159 sensors have been installed, as shown in Fig. 3.

2.2 Stage 1: MLP development

The MLP employs a four hidden layer architecture with an input layer of 4 features and an output layer that progressively reduces the number of neurons from input features to air temperature prediction. The choice of 128 neurons in the first hidden layer follows the common heuristic of having the first hidden layer size as a power of 2 between 2-5 times the number of inputs [20]. This architecture size has proven effective in similar atmospheric and environmental prediction tasks where the relationship between inputs and outputs involves multiple non-linear interactions [21].

Dropout is one of the most popular regularization methods for preventing neural network models from overfitting in the training phase [22]. 20% dropout is applied to the first 2 hidden layers. The Rectified Linear Unit (ReLU) activation function is used throughout the hidden layers. ReLU provides computational efficiency and addresses the vanishing gradient problem that affects traditional activation functions in deep networks [23]. The output layer employs linear activation, appropriate for continuous temperature prediction.

The MLP model follows the common 70-15-15 split for training, validation and testing sets [21]. The model's weights are updated during training using Adam optimizer, which adapts the learning rate for each weight individually and incorporates momentum, which helps the optimization process continue moving in productive directions and avoid getting stuck in local minima [24]. A learning rate of 0.001 is used in weight updates, which is a widely tested starting point that provides stable convergence for neural networks across various applications [25]. The model uses a batch size of 32, as it provides a sufficient gradient averaging to smooth out the randomness inherent in individual samples [26]. The model trains for a maximum of 200

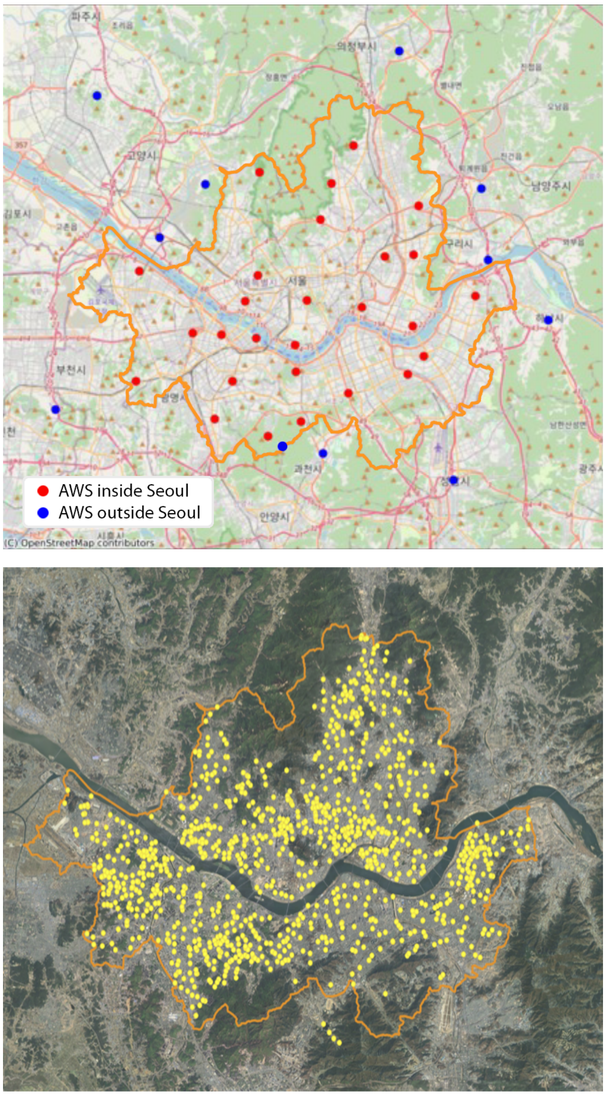

Figure 3. Location of AWS weather stations (top) and S-DoT sensors (bottom)

epochs, with an early stopping patience of 20 epochs to avoid overfitting.

2.3 Stage 2: Independent Testing with S-DoT Sensors

The independent testing begins after the MLP model has completed training using the AWS data. The trained model generates air temperature predictions at each S-DoT sensor location, and these are then directly compared with the actual air temperature measurements from the S-DoT sensors at 11:00 AM. The S-DoT sensors are more densely distributed across Seoul, which provides a spatial testing that the sparse AWS cannot provide. The dense network captures microclimate variations within the urban environment, testing the model's ability to predict air temperatures at locations far from any training stations.

3 Results

The MLP model for converting LST to air temperature was developed, validated and tested using AWS data (2013–2024) as ground truth and further tested using the S-DoT sensor data (2020–2024).

3.1 MLP model performance

Figure 4 shows the model training loss, showing how well the model fits the training data with each epoch, as well as the validation loss, which shows the model's performance on the held-out validation set. Both curves show successful learning behavior, as they decrease rapidly in early epochs as the model learns patterns, then gradually stabilize around the 25th epoch. The convergence of both training and validation curves at similar loss values indicates successful training without overfitting. The early stopping was activated at epoch 71 when validation loss showed no improvement for 20 consecutive epochs.

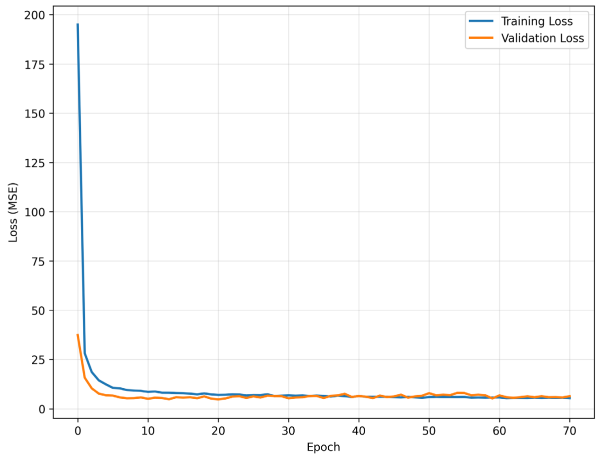

Figure 4. Training and validation loss curves during MLP development

The performance of the model is quantified in Table 1. The coefficient of determination (R^2) value of 0.968 indicates a well-captured nonlinear relationship between LST and air temperature. The performance of this MLP aligns with recent studies in urban temperature estimation, where Salih et al. [13]'s MLP model obtained an R^2 of 0.91. The Root Mean Square Error (RMSE) of 2.1°C is also in a similar range compared to other papers, where Choi et al. [12] got RMSE of 2.19°C using an artificial neural network (ANN). Finally, the Mean Absolute Error (MAE) of 1.62°C provides the average absolute difference between predicted and actual air temperatures.

Table 1. MLP performance metrics for each of the two stages

Data	Period	R^2	RMSE	MAE
AWS	2013–2024	0.968	2.10°C	1.62°C
S-DoT	2020–2024	0.807	4.73°C	3.87°C

3.2 Independent S-DoT testing results

The trained MLP model is further tested with independent S-DoT sensors for the period 2020–2024. Figure 5 shows the predicted versus observed air temperatures at S-DoT sensor locations, with points clustering along the 1:1 line. The mean difference is 0.98°C, with a standard deviation of 4.63°C. The performance of the model during independent testing (Table 1) is lower than for the validation test set, though the R^2 value of 0.807 still indicates a reasonable predictive capability. This is in spite of the fact that S-DoT sensors, unlike AWS, are not installed according to meteorological standards, adding to the uncertainty in their measurements.

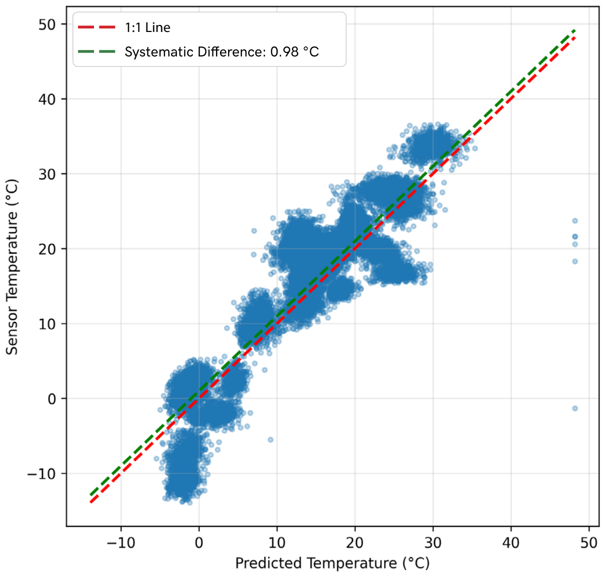

Figure 5. Predicted air temperature testing with S-DoT sensors (2020-2024)

3.3 Model application: Air temperature maps

Figure 6 shows a scatter plot of the measured LST from the satellite images and the predicted air temperature (AT) from the MLP model during the 12-year analysis period. The results show that the difference between LST and AT increases as the measured LST increases. This aligns with Naserikia et al. [27]'s findings, which observed greater temperature differences between LST and air temperature in built environments during warm days.

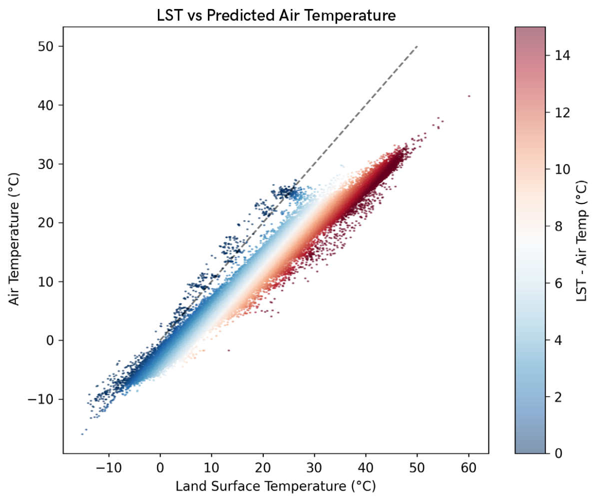

Figure 6. Scatter plot of land surface temperature and final predicted air temperature for the period 2013–2024

As shown in Table 2, the LST tends to be much larger than AT in the summer, with mean differences ranging from 3.94°C in winter to 12.24°C in summer. The larger summer difference reflects intense solar heating of urban surfaces during peak radiation hours, while winter's lower sun angle and reduced radiation result in smaller differences. This consistent seasonal pattern validates the model's physical realism and demonstrates that the MLP successfully captures the varying thermal relationships throughout the year. The finalized model is used to generate air temperature distributions based on LST, as shown in the maps in Fig. 7.

Table 2. Difference between land surface temperature and final predicted air temperature

Metric	Value
Mean Temperature Difference	7.78°C
Spring	9.40°C
Summer	12.24°C
Fall	7.51°C
Winter	3.94°C
Median Temperature Difference	7.58°C
Standard Deviation	3.88°C

4 Conclusions

The research successfully developed a Multi-Layer Perceptron model to convert satellite-based Land Surface Temperature (LST) to air temperature using Normalized Difference Vegetation Index (NDVI), Digital Elevation Model (DEM) and Solar Zenith Angle (SZA) us-

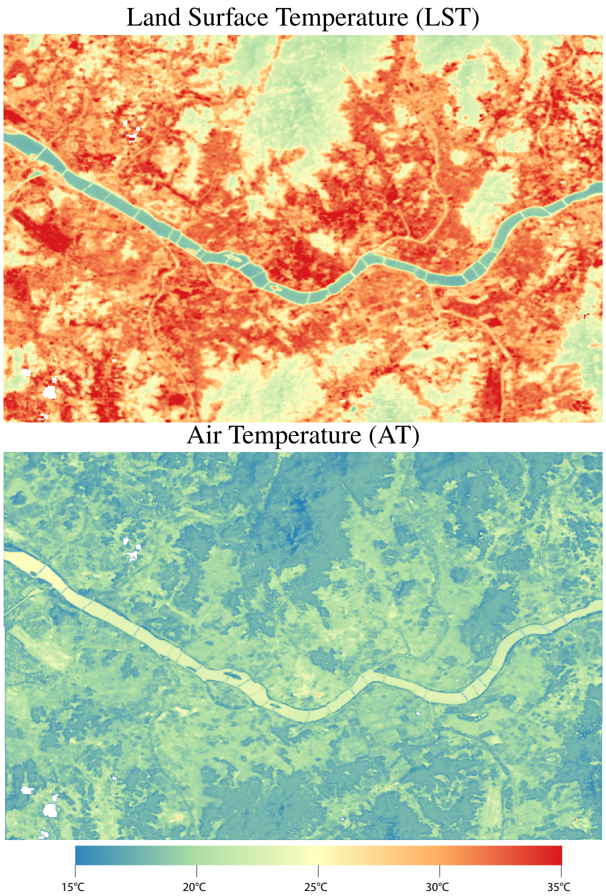

Figure 7. Land surface temperature and predicted air temperature on 25th May 2022 11:10:19

ing air temperature data from Automatic Weather Stations (AWSs) as ground truth data. The MLP model achieved an R^2 of 0.968 and tested with independent S-DoT sensor data. The independent testing was conducted using data from 1000+ S-DoT weather sensors for the period 2020–2024, achieving a mean temperature difference was 0.98°C and an R^2 of 0.807, confirming that satellite imagery provides a reliable method for urban temperature monitoring when ground-based stations are limited.

However, it is important to acknowledge that the analysis uses single hourly temperature observations, since Landsat provides only 1-2 images per month at a fixed time of 11:12 AM. Future research should focus on the development of methods to model diurnal variations in temperature distributions. The use of more frequent satellite observations, if available, could better capture temporal scales to demonstrate the cascading effects from urban form through temperature to energy consumption. Furthermore, more advanced machine learning methods or hybrid approaches combining satellite images with physical models to capture diurnal patters should be explored.

Despite these limitations, the decade-long analysis provides valuable insights into the spatial patterns and long-term trends that inform urban planning strategies. While many researchers have tried to use satellite imagery for urban temperature analysis, few have validated their models with an independent data source. The testing using S-DoT sensors, based on over 23,000 data points from a dense sensor network, shows that satellite-based approaches can accurately convert data to air temperature. Unlike most urban studies that analyze data over a short period, this research examines a full decade of data from 2013 to 2024.

The findings from this research provide specific, quantitative guidance for urban planning policies aimed at mitigating air temperature and managing energy consumption in dense urban districts.

References

[1] J.W. Oh, J. Ngarambe, P.N. Duhirwe, G.Y. Yun, and M. Santamouris. Using deep-learning to forecast the magnitude and characteristics of urban heat island in Seoul Korea. *Scientific Reports*, 10:3559, 2020. doi:10.1038/s41598-020-60632-z.

[2] D. Maiullari. *Urban form influence on microclimate and building cooling demand: An analytical framework and its application in the Rotterdam case*. PhD thesis, Delft University of Technology, 2023.

[3] M. Mosteiro-Romero and Schlueter A. Effects of occupants and local air temperatures as sources of stochastic uncertainty in district energy system modeling. *Energies*, 14:2295, 2021. doi:10.3390/en14082295.

[4] J. Voogt and T. Oke. Thermal remote sensing of urban climates. *Remote Sensing of Environment*, 86:370– 384, 2003. doi:10.1016/s0034-4257(03)00079-8.

[5] J. Schatz and C. J. Kucharik. Urban climate effects on extreme temperatures in Madison, Wisconsin, USA. *Environmental Research Letters*, 10:094024, 2015. doi:10.1088/1748-9326/10/9/094024.

[6] H. Meyer, M. Katurji, T. Appelhans, M. Müller, T. Nauss, P. Roudier, and P. Zawar-Reza. Mapping daily air temperature for Antarctica based on MODIS LST. *Remote Sensing*, 8:732, 2016. doi:10.3390/rs8090732.

[7] P. Noi, J. Degener, and M. Kappas. Comparison of multiple linear regression, cubist regression, and random forest algorithms to estimate daily air surface temperature from dynamic combinations of MODIS LST data. *Remote Sensing*, 9:398, 2017. doi:10.3390/rs9050398.

[8] Y. Chen, J. Quan, W. Zhan, and Z. Guo. Enhanced statistical estimation of air temperature incorporating nighttime light data. *Remote Sensing*, 8:656, 2016. doi:10.3390/rs8080656.

[9] M. Ignatius, J. Lim, B. Gottkehaskamp, K. Fujiwara, C. Miller, and F. Biljecki. Digital twin and wearables unveiling pedestrian comfort dynamics and walkability in cities. *ISPRS Ann. Photogramm. Remote Sens. and Spatial Inf. Sci.*, X-4/W5-2024:195–202, June 2024. doi:10.5194/isprs-annals-X-4-W5-2024-195-2024.

[10] X. Ding, Y. Zhao, Y. Fan, Y. Li, and J. Ge. Machine learning-assisted mapping of city-scale air temperature: Using sparse meteorological data for urban climate modeling and adaptation. *Building and Environment*, 234:110211, 2023. doi:10.1016/j.buildenv.2023.110211.

[11] K. Tang, H. Zhu, and P. Ni. Spatial downscaling of land surface temperature over heterogeneous regions using random forest regression considering spatial features. *Remote Sensing*, 13:3645, 2021. doi:10.3390/rs13183645.

[12] S. Choi, D. Jin, N. Seong, D. Jung, S. Sim, J. Woo, U. Jeon, Y. Byeon, and K. Han. Near-surface air temperature retrieval using a deep neural network from satellite observations over South Korea. *Remote Sensing*, 13:4334, 2021. doi:10.3390/rs13214334.

[13] W. Salih, E. M. E. Khalki, V. Ongoma, R. Lguensat, B. Aithssaine, H. Ouatiki, F. Driouech, B. Sebbar, S. Achli, and A. Chehbouni. TEMLI: A high-resolution air temperature estimation using machine learning and land surface data across Morocco. *Earth Systems and Environment*, 9:1311–1331, 2025. doi:10.1007/s41748-025-00629-8.

[14] T. Kotsiopoulos, P. Sarigiannidis, D. Ioannidis, and D. Tzovaras. Machine learning and deep learning in smart manufacturing: The smart grid paradigm. *Computer Science Review*, 40:100341, 2021. doi:10.1016/j.cosrev.2020.100341.

[15] W. Liao, T. Hong, and Y. Heo. The effect of spatial heterogeneity in urban morphology on surface urban heat islands. *Energy and Buildings*, 244:111027, 2021. doi:10.1016/j.enbuild.2021.111027.

[16] S. Raj and G. Y. Yun. Exploring the role of strategic urban planning and greening in decreasing surface urban heat island intensity. *Journal of Asian Architecture and Building Engineering*, 24:866–879, 2024. doi:10.1080/13467581.2024.2308592.

[17] N. Sahani. Assessment of spatio-temporal changes of land surface temperature (LST) in Kanchenjunga Biosphere Reserve (KBR), India using Landsat satellite image and single channel algorithm. *Remote Sensing Applications: Society and Environment*, 24: 100659, 2021. doi:10.1016/j.rsase.2021.100659.

[18] Korea Meteorological Administration. KMA data service. `https://data.kma.go.kr/cmmn/main.do`, 2025. Accessed: 11/09/2025.

[19] M. Park and K. Baek. Quality management system for an IoT meteorological sensor network–Application to Smart Seoul Data of Things (S-DoT). *Sensors*, 23:2384, 2023. doi:10.3390/s23052384.

[20] J. Heaton. *Introduction to Neural Networks with Java*. Heaton Research, USA, 2008.

[21] S. Rasp, M. S. Pritchard, and P. Gentine. Deep learning to represent subgrid processes in climate models. *Proceedings of the National Academy of Sciences*, 115:9684–9689, 2018. doi:10.1073/pnas.1810286115.

[22] I. Salehin and D. Kang. A review on dropout regularization approaches for deep neural networks within the scholarly domain. *Electronics*, 12:3106, 2023. doi:10.3390/electronics12143106.

[23] X. Glorot, A. Bordes, and Y. Bengio. Deep sparse rectifier neural networks. In *Proceedings of the 14th International Conference on Artificial Intelligence and Statistics (AISTATS)*, 2011.

[24] D. P. Kingma and J. L. Ba. Adam: A method for stochastic optimization. In *Proceedings of the 3rd International Conference for Learning Representations*, 2015. doi:10.48550/arxiv.1412.6980.

[25] Y. Bengio. Practical recommendations for gradient-based training of deep architectures. In *Neural Networks: Tricks of the Trade*, pages 437–478. Springer, Berlin, Heidelberg, 2012. doi:10.1007/978-3-642-35289-8_26.

[26] D. Masters and C. Luschi. Revisiting small batch training for deep neural networks. *arXiv preprint*, 1804.07612, 2018. doi:10.48550/arxiv.1804.07612.

[27] M. Naserikia, M. A. Hart, N. Nazarian, B. Bechtel, M. Lipson, and K. A. Nice. Land surface and air temperature dynamics: The role of urban form and seasonality. *The Science of the Total Environment*, 905: 167306, 2023. doi:10.1016/j.scitotenv.2023.167306.